Sensors & Transducers, Vol. 273, Issue 2, June 2026, pp. 21-29

www.sensorsportal.com

Sensors & Transducers

Published by IFSA Publishing, S. L., 2026

http://www.sensorsportal.com

A Study on SiC-MEMS Based Peripheral MOSFET Embedded and Current Mirror Integrated Pressure Sensor for High-Temperature Applications

[1, *] Gaurav KUMAR, [1] Menuvolu TETSEO, [1] Kalpana GOGOI, [2] Shashi KUMAR, [1] Pradeep Kumar RATHORE, [3] Kulwant SINGH, [4] Shankar DUTTA and [5] Lolit Kumar SINGH

[1] Department of Electronics and Communication Engineering, National Institute of Technology Meghalaya, Sohra, 793108, Meghalaya, India

[2] Micron Technology Operation India LLP, Hyderabad, India

[3] Department of Industry 4.0, Skill Faculty Engineering & Technology, Shri Vishwakarma Skill University, Palwal, Haryana, India

[4] Micro-Electro-Mechanical System Division, Solid State Physics Laboratory, Defence Research & Development Organisation (DRDO), Delhi, India

[5] Department of Electronics and Communication Engineering, National Institute of Technology Manipur, Imphal, India

Tel.: +91 9418580400

[*] Gaurav.kumar@nitm.ac.in

Received: 17 Feb. 2026 /Revised: 23 March 2026 /Accepted: 15 May 2026 /Published: 29 June 2026

Abstract: This paper presents a design and simulation study of SiC-MEMS pressure sensors featuring an embedded peripheral MOSFET and an integrated current-mirror for high temperature applications. The proposed pressure sensor structures employ square and circular shaped strain sensing MOSFETs embedded on the periphery of square and circular SiC diaphragms, respectively. The MOSFETs are configured as a resistively loaded current mirror configuration. Pressure-induced strain is detected through the piezoresistive behaviour of 4H-SiC n-channel MOSFET devices. The mechanical and electrical behaviour of the proposed sensors was simulated using COMSOL Multiphysics and TSPICE software over pressure and temperature ranges of 0 – 10 MPa and 25 – 400 °C, respectively. The simulated pressure sensitivities for square and circular sensors were found to be 0.2 mV/MPa and 0.4 mV/MPa, respectively, at 25 °C which increased to 27.86 mV/MPa and 62.66 mV/MPa at 400 °C. The temperature sensitivities of proposed square and circular shaped pressure sensors were found to be 0.65 mV/ °C and 1.49 mV/ °C, respectively, at an applied pressure of 10 MPa. The simulation results underscore the critical role of channel geometry in improving sensor sensitivity, paving the way for robust 4H-SiC MOS-based pressure sensors for harsh environments.

Keywords: Silicon carbide, MOSFET, MEMS, Pressure sensor, Piezoresistivity, Current mirror, Diaphragms.

1. Introduction

Pressure is a critical physical parameter widely utilized in consumer electronics, medical, aerospace, automotive, industrial and defence applications [1]. Advancements in semiconductor and Micro-Electro-Mechanical Systems (MEMS) technologies have enabled the integration of complex mechanical components such as beams, flexures, linkages, sensing units, and actuators onto a single microchip [2-7].

Among MEMS structures, the diaphragm is the most fundamental micromechanical element and is widely used in pressure sensors. When subjected to pressure, a diaphragm deflects and this deflection can be measured by piezoresistive [8], piezoelectric [9], capacitive [10], or optical methods [11]. However, each technique has its limitations, especially under harsh environmental conditions [12]. The MOSFET embedded sensing technique enables the development of CMOS-MEMS integrated sensors by offering a novel transduction mechanism based on the piezoresistive characteristics of MOSFETs [13].

Researchers from all across the world are attempting to optimise silicon transistors for pressure measurement in order to boost sensitivity and reduce device size and minimize the mechanical and electrical faults [14-16]. However, high temperatures have an impact on silicon device performance, limiting their use in extremely harsh environments [17]. MEMS pressure sensors based on silicon carbide (SiC) have become a possible substitute for silicon because of their low intrinsic carrier concentration, strong breakdown field strength, and broad bandgap (3 eV), which make them appropriate for high temperature applications [18]. The piezoresistive properties of SiC have been widely explored by researchers for pressure sensing applications in harsh environments [19-21].

In our earlier work [22], a conceptual and simulation study was conducted on a SiC-MEMS pressure sensor integrating a conventional rectangular MOSFET-based strain sensing element, a current mirror readout circuit and a SiC diaphragm, representing one of the earliest reports on SiC-based MOSFET embedded pressure sensors with current mirror readout. The sensor employed two smaller strain sensing MOSFETs at the diaphragm's edge and centre to sense tensile and compressive stresses under applied pressure. This work extends our previous study by proposing pressure sensors with a single square or circular MOSFET at the periphery of square or circular SiC diaphragms to exploit maximum edge stresses. This paper presents background and related work in Section 1, sensor structure and operation in Section 2, followed by simulation results in Section 3, design of mask layout and fabrication steps in Section 4, and finally concludes in Section 5.

2. Sensor Structure and Working Principle

This study investigates two pressure sensor structures that employ square and circular shaped strain sensing MOSFETs embedded on the periphery of square and circular SiC diaphragms, respectively. The MOSFETs are arranged in a current mirror configuration with resistive loads, as shown in Fig. 1(a) and 1(b). Fig. 1(c) and 1(d) present the cross-sectional views of square and circular strain-sensitive MOSFETs integrated along the edges of the SiC diaphragms. Identical current-mirror pairs (M1–M2) are used in each design, with M1 as the reference and sensing transistor, M2, is integrated on a flexible SiC diaphragm that bends when external pressure is applied, modulating carrier mobility in the channel and consequently altering the drain current. This variation produces a pressure-dependent output voltage across the drains of the current-mirror circuit. Table 1 presents the fundamental governing equations of the proposed SiC-MEMS based peripheral MOSFET embedded and current mirror integrated pressure sensors.

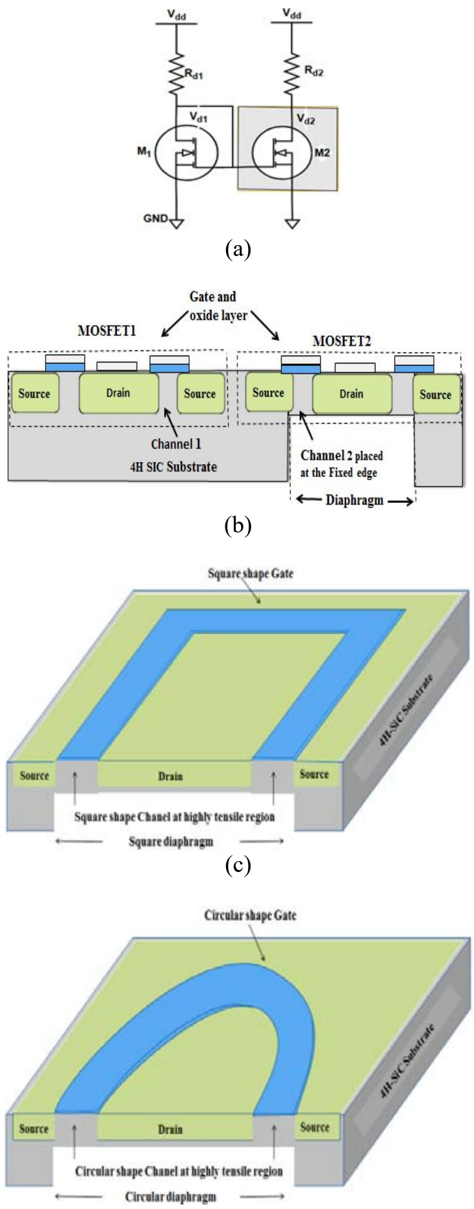

Fig. 1. (a) Schematic of a resistively loaded n-channel MOSFET current mirror circuit with the reference transistor M1 and the pressure-sensitive transistor M2, (b) Cross-sectional view of the SiC-based MOSFET integrated pressure sensor structure, (c) Cross-sectional view of the square shaped MOSFET-based sensor, (d) Cross-sectional view of the circular shaped MOSFET-based sensor.

Table 1. Fundamental governing equations of the proposed SiC-MEMS based peripheral MOSFET embedded and current mirror integrated pressure sensors.

A. Mechanical pressure sensing elements: Square and circular diaphragms [23]		
Diaphragm shape	**Maximum displacement**	**Maximum stress**
Square	$0.26pa^4\frac{(1-\nu^2)}{Eh^3}$	$1.23p\frac{a^2}{h^2}$
Circular	$0.19pa^4\frac{(1-\nu^2)}{Eh^3}$	$0.75p\frac{a^2}{h^2}$
B. Transduction mechanism: Piezoresistive effect in MOSFET [24]		
$\frac{\Delta\mu}{\mu} = -\frac{\Delta R}{R} = -(\pi_l\sigma_l + \pi_t\sigma_t)$		
C. Current mirror readout circuit		
$V_{OUT} = V_{D1} - V_{D2} = (I_{D2} - I_{D1})R_D$, $I_{D1} = \mu C_{ox}\frac{W}{L}\frac{(V_{gs}-V_t)^2}{2}$, $I_{D2} = (\mu+\Delta\mu)C_{ox}\frac{W}{L}\frac{(V_{gs}-V_t)^2}{2}$, where p is the applied pressure, a is the side length or radius and h indicates the thickness of square and circular diaphragm, E and ν denotes the Young's modulus and Poisson's ratio of the diaphragm material, μ and R are the initial electron mobility and channel resistance, Δμ and ΔR are the changes in electron mobility and channel resistance under applied pressure, π_l, π_t, σ_l and σ_t denotes the longitudinal and transverse piezoresistive and stress components, RD is the drain resistance, ID1, ID2, VD1 and VD2 are the drain current and voltages of reference and pressure sensing MOSFETs.		

The design and simulation parameters used for the proposed SiC-MEMS pressure sensor embedded peripheral MOSFET and integrated current mirror are given in Table 2. In the first pressure sensing structure, a square shaped SiC strain sensing MOSFET with its channel integrated along the periphery of a square SiC diaphragm. Similarly, for the second sensor structure, a circular shaped SiC strain sensing MOSFET with its channel integrated along the periphery of circular SiC diaphragm. The simulations of mechanical and electrical performance were carried out using COMSOL Multiphysics and TSPICE.

3. Results and Discussion

To investigate the piezoresistive behaviour of square and circular shaped n-channel SiC MOSFET pressure sensing structures, a three-dimensional finite element model consisting of an n-channel MOSFET equivalent piezoresistive embedded in SiC diaphragm was developed using COMSOL Multiphysics. The temperature-dependent electrical behavior of the n-channel 4H-SiC MOSFET, as reported in [26], was assumed to align with standard current-mirror-based pressure sensing designs. At room temperature, a voltage equivalent to the MOSFET Early voltage was applied across the corresponding piezoresistor, and this voltage was used exclusively to simulate the sensor's piezoresistive behaviour in COMSOL Multiphysics. To evaluate the device response under applied stress, pressure was applied on the diaphragm. Fig. 2(a) illustrates the three-dimensional square-shaped pressure sensing structure modelled in COMSOL Multiphysics, while Fig. 2(b) depicts the corresponding stress distribution in the square diaphragm under externally applied pressure of 10 MPa. The stress profile is visualized using a color gradient, where purple represents regions of minimum stress and red indicates areas of maximum stress. Similarly, Fig. 3 shows the three-dimensional circular-shaped pressure-sensing structure and stress distribution in the circular diaphragm subjected to 10 MPa of applied pressure.

Table 2. Parameters used for design and simulation of the proposed SiC-MEMS based pressure sensor featuring a peripheral embedded MOSFET and a current-mirror readout circuit.

Parameter	Unit	Square Shape	Circular Shape
A. Parameters for analyzing Piezoresistive Effects in N-Channel 4H-SiC MOSFETs using COMSOL Multiphysics.			
Diaphragm dimensions (side/diameter, thickness)	μm	100, 2.5	110, 2.5
MOSFET equivalent piezoresistor value	kΩ	13852	13852
Piezoresistive coefficients [25] ($\times 10^{-11}$)	Pa^{-1}	$\pi_{11} = -3.4$, $\pi_{12} = 6.15$	$\pi_{11} = -3.4$, $\pi_{12} = 6.15$
B. Parameters for analyzing electrical behavior of Current Mirror Design using TSpice software.			
MOSFET dimensions (L, W)	μm	10, 300	10, 300
Early voltage	(V/μm)	33	33
Oxide capacitance (Cox)	fF/μm^2	4.425	4.425
Gate Oxide thickness (tox)	nm	20	20
Threshold Voltage(Vth)	V	2.69	2.69
Carrier mobility (μ)	cm^2/Vs	0.0248	0.0248
Gate-to-source voltage, VGS	V	20	20
Drain resistor, RD	kΩ	10	10
Reference current, I_{ref}	μA	23.8255	23.8255

The simulation results reveal that the maximum stress is concentrated around the clamped edges of the diaphragm, reaching 5661 MPa for the square diaphragm and 5371 MPa for the circular diaphragm. This confirms that the square diaphragm experiences greater stress concentration at its fixed boundaries under the applied pressure. To assess the accuracy and reliability of the simulation results for the 4H-SiC MOSFET-based piezoresistive sensor, a mesh convergence analysis was performed in COMSOL Multiphysics for both circular and square piezoresistor configurations under a uniform applied pressure of 10 MPa.

Nine different mesh sizes were employed to assess model sensitivity and convergence. The simulation results for the square and circular geometries are summarized in Table 3. Fig. 4 shows the variation in resistance of square and circular MOSFET-equivalent piezoresistors with different default mesh settings in COMSOL Multiphysics. In both cases, the resistance values are nearly saturated as the mesh is refined from finer to extremely fine. Based on this convergence, the finer mesh setting was chosen for simulations to balance accuracy and computational efficiency.

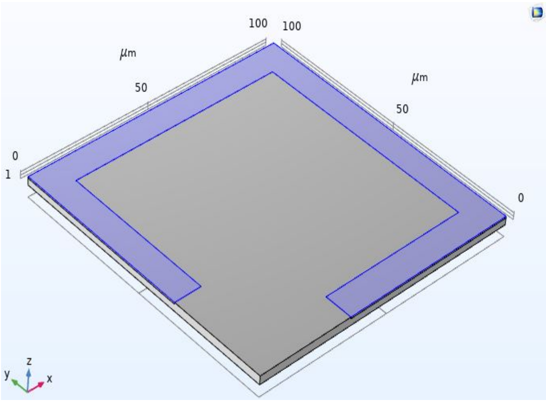

(a)

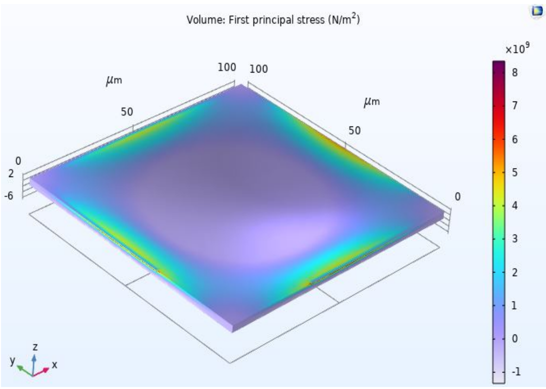

(b)

Fig. 2. (a) Three-dimensional square shaped pressure sensing structure integrated with a square shaped MOSFET equivalent piezoresistor, and (b) Stress distribution at an applied pressure of 10 MPa.

Fig. 5(a) depicts channel resistance versus applied pressure (0–10 MPa) for square and circular 4H-SiC MOSFETs. MOSFET M1, located at the fixed edge, exhibits a constant channel resistance of 13.85 MΩ, indicating no pressure sensitivity. In contrast, MOSFET M2 devices with square and circular channels, embedded near the fixed edge, experience longitudinal channel stress under applied pressure, resulting in pressure-dependent resistance reduction. At 10 MPa, the channel resistance decreases to 13.70 MΩ for the square channel and 13.56 MΩ for the circular channel. Fig. 5(b) depicts the effect of externally applied pressure on the channel mobility of the current mirror transistor (M2), whereas the reference transistor (M1) retains a constant mobility of 0.0248 $cm^2/V\cdot s$, indicating no pressure dependence. In contrast, the pressure-sensitive MOSFETs M2 with square and circular channels exhibit a noticeable increase in channel mobility with rising pressure, reaching 0.0251 $cm^2/V\cdot s$ and 0.0253 $cm^2/V\cdot s$, respectively. The simulated drain current and channel resistance under zero pressure show good agreement with COMSOL results. The pressure response of M2 was further analysed using FEM modelling. For input pressure of 10 MPa, an increase of nearly 0.2 µA is observed in the drain current for the square shaped channel and 0.41 µA for the circular channel configuration, which are then converted to voltage signals using the drain resistance R_D, as shown in Fig. 1(a).

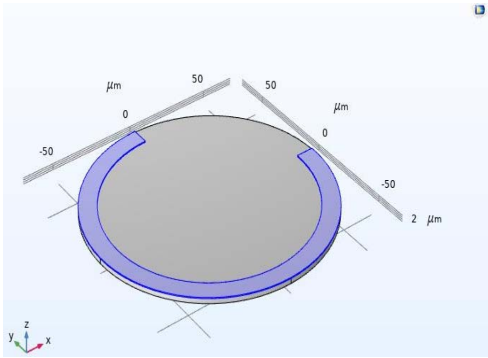

(a)

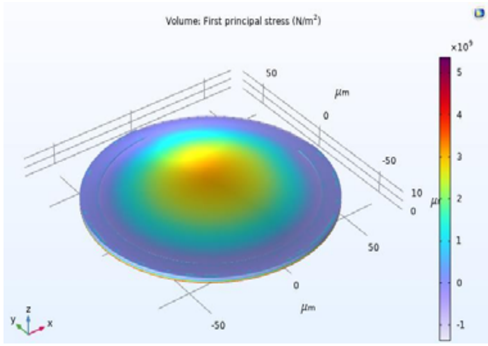

(b)

Fig. 3. (a) Three-dimensional circular shaped pressure sensing structure integrated with a circular shaped MOSFET equivalent piezoresistor, and (b) Mechanical stress distribution under an applied pressure of 10 MPa.

Table 3. Results of mesh analysis for circular and square-shaped MOSFET equivalent piezoresistor.

Default mesh size in COMSOL Multiphysics	MOSFET equivalent piezoresistance (MΩ)	
	Circular shaped	Square shaped
Extremely coarse	13.347	13.70
Extra coarse	13.362	13.741
Coarser	13.415	13.768
Coarse	13.510	13.809
Normal	13.560	13.839
Fine	13.670	13.855
Finer	13.728	13.8601
Extra fine	13.745	13.86302
Extremely fine	13.758	13.86417

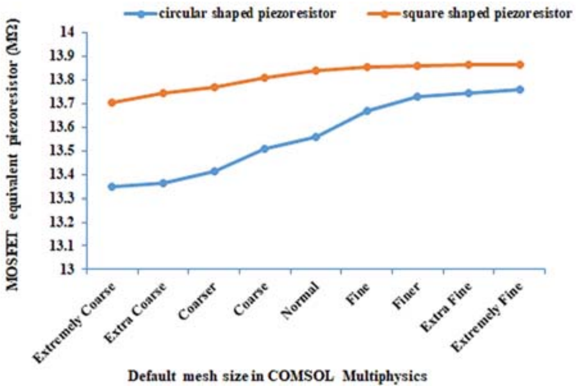

Fig. 4. Variation in MOSFET equivalent piezoresistance as a function of mesh size for square and circular shaped piezoresistors.

As illustrated in Fig. 6, the drain output voltages of both the reference and pressure-sensitive MOSFETs change in response to the applied pressure for square and circular channel geometries placed near the diaphragm's edge, The drain voltage exhibits a continuous decline as the applied pressure rises to 10 MPa. Under ambient conditions (25 °C and 10 MPa), the differential output voltages $V_{D1} - V_{D2}$ for the square and circular peripheral MOS devices are approximately 2 mV and 4.17 mV, respectively. Fig. 7 presents the output response of the proposed peripheral MOS-embedded SiC-MEMS pressure sensors at a raised temperature of 400 °C. Due to the excellent temperature endurance and robustness of 4H-SiC in extreme environments, the proposed sensor has an almost linear voltage response with increasing temperature under constant pressure conditions.

The output voltages of the square and circular shaped peripheral MOSFET embedded pressure sensors reach approximately 278.5 mV and 626.6 mV, respectively. This consistent increase in output voltage with temperature indicates reliable device operation and confirms its ability to maintain stable performance at elevated temperatures, thereby validating the suitability of the proposed design for harsh-environment sensing applications. Figs. 8 and 9 illustrate the output voltage response of the square and circular shaped SiC MOSFET-based pressure sensors as a function of input pressure applied in the range of 0 to 10 MPa over a temperature span of 25 °C to 400 °C. The results show that the sensor's output voltage exhibits a linear dependence on input applied pressure across the full range of temperature from 25 °C to 400 °C.

4. Proposed Mask Layout and Fabrication Process Flow

This section proposes design of mask layout and step by step fabrication process flow for the development of proposed 4H-SiC MOSFET-based pressure sensors. As illustrated in Figs. 10, the fabrication of proposed SiC based pressure sensors employ six-mask-layer design, following a "CMOS-First" and "MEMS-Last" integration strategy. The proposed pressure sensor chip, with dimensions of 620 × 620 μm, was designed using K-Layout software. The fabrication process flow for the proposed pressure sensors was designed based on established literature on fabrication of SiC based MOSFET and bulk micromachining techniques of SiC substrate [26–28]. Fig. 11. illustrates the sequential fabrication process of the proposed 4H-SiC n-channel MOSFET device.

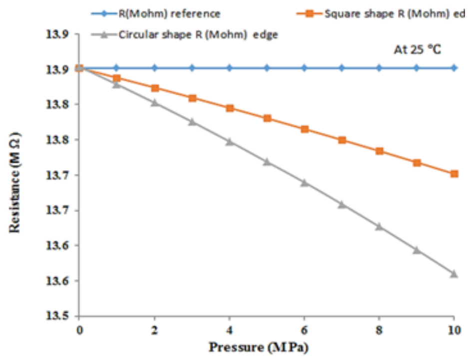

(a)

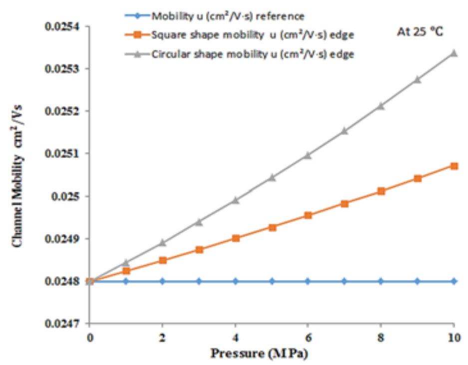

(b)

Fig. 5. Pressure-dependent characteristics showing (a) channel resistance and (b) carrier mobility for square- and circular shaped sensing MOSFETs as a function of pressure.

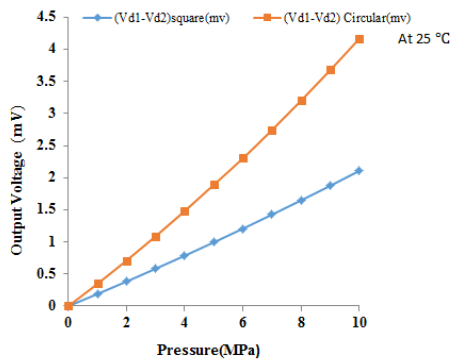

Fig. 6. Pressure-dependent output voltage characteristics at 25 °C, exhibiting pressure sensitivities of approximately 0.21 and 0.41 mV/MPa, respectively, for the square and circular shaped SiC MOS based pressure sensors as a function of pressure.

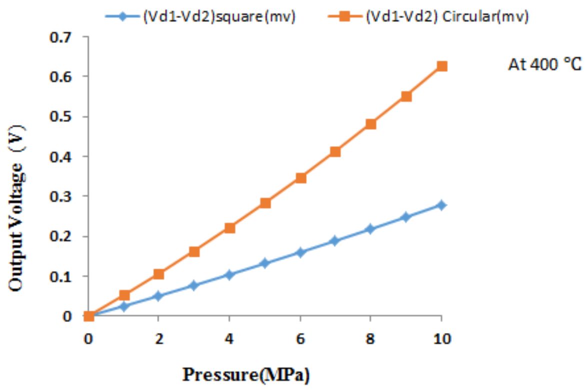

Fig. 7. Output voltage characteristics of square and circular SiC MOSFET-based pressure sensors at 400 °C, showing pressure sensitivities of approximately 27.86 and 62.62 mV/MPa, respectively.

The details of the proposed fabrication process flow are outlined below:

a) The fabrication of the sensor begins with a properly cleaned p-type 4H-SiC substrate;
b) A thick SiO_2 field oxide layer is deposited to provide surface isolation;
c) The first photolithography step defines the source and drain regions;
d) Arsenic ion implantation is performed to achieve n-type doping in these regions;
e) Dopant activation is carried out through post-implantation annealing, during which a carbon cap is employed to prevent surface degradation;
f) The carbon cap is subsequently removed;
g) A thin gate oxide is grown by thermal oxidation'
h) The second photolithography step patterns the contact vias for the source and drain, followed by Nb/Ni deposition to form low-resistance ohmic contacts;
i) Source and drain contacts are formed using a lift-off process;
j) Metal silicidation is performed to further reduce contact resistance;
k) An aluminum layer is deposited over the structure;
l) The third photolithography step patterns the aluminum layer to form the gate electrode and contact pads for the source, drain and gate;
m) An interlayer SiO_2 dielectric is deposited to electrically isolate the metal layers;
n) The fourth photolithography step, followed by dielectric etching, opens the contact windows;
o) A second aluminum layer is deposited for final metallization;
p) Photoresist is applied to both sides of the wafer;
q) The fifth photolithography step defines the backside oxide window to enable diaphragm formation;
r) The diaphragm is realized through backside bulk micromachining of the 4H-SiC substrate;
s) Photoresist is removed from both sides of the wafer;
t) The sixth photolithography step patterns the top metal interconnects and contact pads.

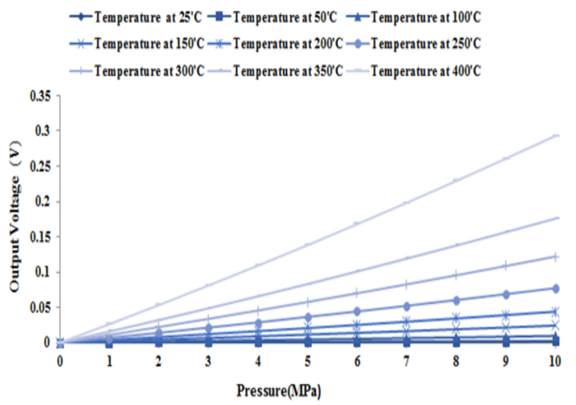

Fig. 8. Variation in the output voltage of square shaped pressure sensor as a function of applied pressure at various temperatures ranging from 25 **°C** to 400 **°C**.

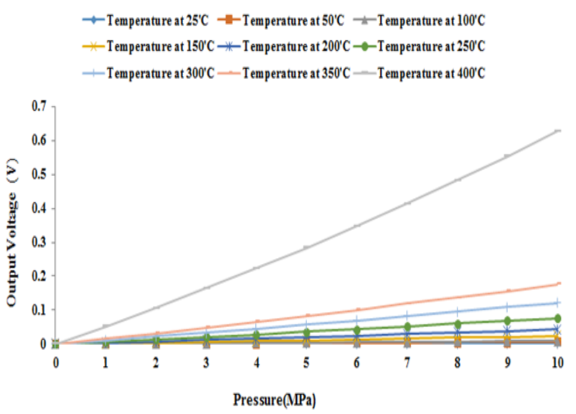

Fig. 9. Variation in the output voltage of circular shaped pressure sensor as a function of applied pressure at various temperatures ranging from 25 °C to 400 °C.

The proposed sensors exhibit competitive sensitivity, demonstrating their suitability for high-temperature pressure sensing. Table 4 compares their sensitivity with previously reported works, highlighting improved performance. Table 5 summarizes important parameters such as chip size, operating pressure range, full-scale output, linearity deviation, and sensitivity at both room temperature and 400 °C.

The observed improvement in sensitivity at elevated temperatures can be attributed to temperature-dependent device characteristics. At higher temperatures, reduced interface trap occupancy and diminished Coulomb scattering enhance the effective channel mobility, as reported in [29–33]. Furthermore, the decrease in threshold voltage with increasing temperature leads to a higher drain current, which collectively contributes to the enhanced sensitivity.

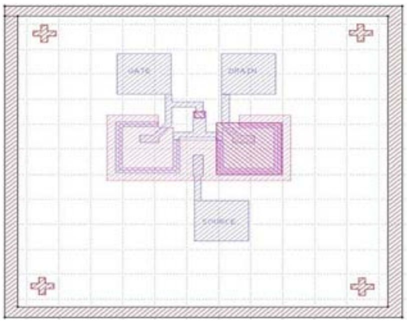

(a)

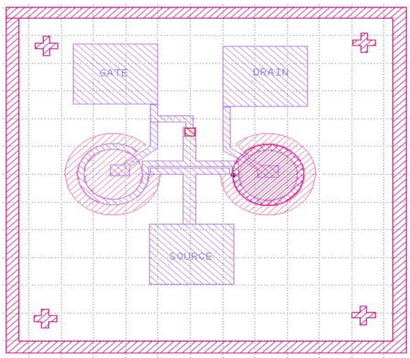

(b)

Fig. 10. Mask layout design of the proposed square and circular shaped SiC MOSFET embedded pressure sensor featuring an integrated current mirror configuration.

Table 4. Comparison of present work with SiC based pressure sensors reported in literature.

Ref.	Sensitivity (mV/MPa)	Readout circuit	Temperatur e
[34]	15.6	Wheatstone Bridge	30 °C
[35]	3.4	Wheatstone Bridge	500 °C
[36]	13.4	Wheatstone Bridge	600 °C
[37]	2	Wheatstone Bridge	400 °C
This work	27.86 and 62.62	Current mirror	400 °C

5. Conclusions

This article describes the design and simulation based study of a 4H-SiC MEMS pressure sensor integrated with n-channel MOSFETs using square and circular shaped channel geometries connected in a current mirror configuration. The proposed pressure sensor structures employ square and circular shaped strain sensing MOSFETs embedded on the periphery of square and circular SiC diaphragms, respectively. The sensor converts strain-induced variations into electrical signals by exploiting the piezoresistive properties of 4H-SiC, achieving linear response over a pressure range of 0 – 10 MPa and temperatures up to 400 °C. Simulation results show enhanced pressure sensitivity for the circular-channel design and reduced temperature sensitivity for the square-channel configuration. The CMOS compatible design ensures robust performance in harsh environments, which clearly indicates its potential use in high-temperature applications for the aerospace, automotive, petrochemical, nuclear, and oil & gas sectors.

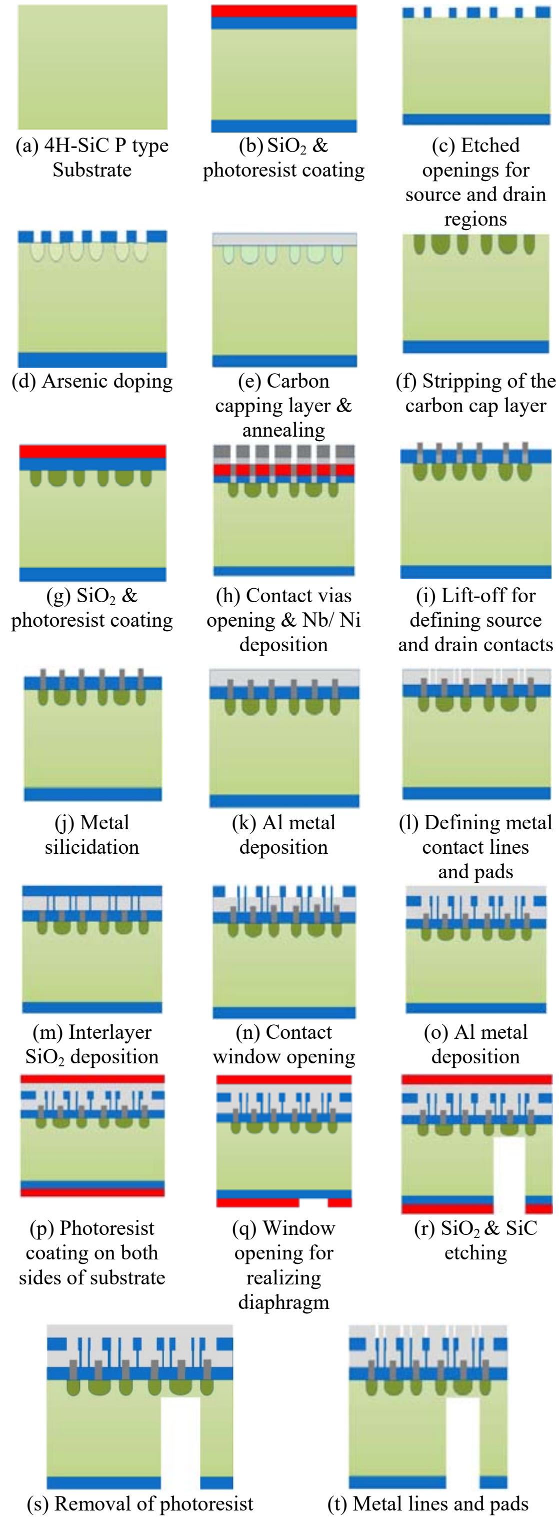

Fig. 11. Design of proposed fabrication process flow of the proposed n-channel 4H-SiC MOSFET based pressure sensor incorporating square and circular channel structures in a current mirror configuration.

Table 5. Key parameters of square and circular shaped SiC-MEMS based Peripheral MOSFET Embedded and Current Mirror Integrated Pressure Sensors.

Parameter	**Unit**	**Square Shape**	**Circular Shape**
A. General Sensor Parameters			
Chip area	μm²	620 × 620	620 × 620
Pressure range	MPa	0-10	0-10
B. Output Characteristics at Different Temperatures			
FSO value measured at 25 °C	mV	2	4.17
FSO value measured at 400 °C	mV	278.5	626.6
Linearity error in FSO at 25 °C	%	2.29	4.14
Linearity error in FSO at 400 °C	%	2.36	4.07
Pressure sensitivity at 25 °C	mV/MPa	0.20	0.416
Pressure sensitivity at 400 °C	mV/MPa	27.86	62.66
C. Thermal Sensitivity and Errors			
Temperature sensitivity at 10 MPa	mV/ °C	0.65	1.49
Error in temperature sensitivity at 1 MPa	μV/ °C	8.27	25.1
Error in temperature sensitivity at 10 MPa	μV/ °C	17.1	64

Acknowledgements

The authors gratefully acknowledge support provided through Project Grant (DFTM/07/3603/DIA-CoE, MZU/MEMS/P-03). The authors also acknowledge the National Institute of Technology Meghalaya for providing institute overhead funds from the DRDO-sponsored project for the payment of publication fees.

References

[1]. X. Han, M. Huang, Z. Wu, Y. Gao, et al., Advances in high performance MEMS pressure sensors: Design, fabrication and packaging, *Microsystems & Nanoengineering*, Vol. 9, Issue 1, 2023, 156.

[2]. E. B. Mansouri, L. M. Middelburg, R. H. Poelma, G. Q. Zhang, et al., High-resolution MEMS inertial sensor combining large proof-mass and integrated capacitive transduction, *Microsystems & Nanoengineering*, Vol. 5, Issue 1, 2019, 60.

[3]. X. He, D. Li, H. Zhou, X. Hui, et al., Theoretical and experimental studies on MEMS variable cross-section cantilever beams for vibration energy harvesting, *Micromachines*, Vol. 12, Issue 7, 2021, 772.

[4]. S. Liao, H. Wang, Z. Li, Design, assembly and simulation of flexure-based modular mechanisms, *Machines*, Vol. 10, Issue 6, 2022, 421.

[5]. X. P. S. Su, H. S. Yang, Design of compliant microleverage mechanisms, *Sensors and Actuators A: Physical*, Vol. 87, Issue 3, 2001, pp. 146-156.

[6]. A. S. Algamili, M. H. Khir, J. O. Dennis, A. Y. Ahmed, et al., A review of actuation and sensing mechanisms in MEMS-based sensor devices, *Nanoscale Research Letters*, Vol. 16, Issue 1, 2021, 16.

[7]. S. Jena, A. Gupta, Review on pressure sensors: A perspective from mechanical to micro-electro-mechanical systems, *Sensor Review*, Vol. 41, Issue 3, 2021, pp. 320-329.

[8]. R. Devi, S. S. Gill, B. Singh, Quantitative analysis of MEMS piezoresistive squared diaphragm pressure sensor for biomedical applications, *Measurement: Sensors*, Vol. 24, 2022, 100522.

[9]. A. Kumar, A. Varghese, A. Sharma, M. Prasad, et al., Recent development and futuristic applications of MEMS based piezoelectric microphones, *Sensors and Actuators A: Physical*, Vol. 347, 2022, 113877.

[10]. K. B. Balavalad, B. G. Sheeparamatti, A critical review of MEMS capacitive pressure sensors, *Sensors & Transducers*, Vol. 187, Issue 4, 2015, pp. 120-129.

[11]. Y. Ge, M. Wang, H. Yan, The principle and architectures of optical stress sensors and the progress on the development of microbend optical sensors, *Advanced Optical Materials*, Vol. 9, Issue 10, 2021, 2001693.

[12]. L. M. Middelburg, W. D. Driel, G. Q. Zhang, From Si towards SiC technology for harsh environment sensing, in Sensor Systems Simulations: From Concept to Solution (W. D. Driel, O. Pyper, C. Schumann, Eds.), *Springer*, Cham, 2020, pp. 1-15.

[13]. N. Wacker, H. Richter, CoMPact modeling of CMOS transistors under uniaxial stress, in *Proceedings of the SAFE Workshop*, 2019, pp. 179-181.

[14]. N. Hafez, S. Haas, K. U. Loebel, D. Reuter, Characterization of MOS transistors as an electromechanical transducer for stress, *Physica Status Solidi A*, Vol. 216, Issue 19, 2019, 1700680.

[15]. M. Basov, Pressure sensor with novel electrical circuit utilizing bipolar junction transistor, in *Proceedings of the IEEE Sensors Conference*, 2021, pp. 1-4.

[16]. L. Ramirez, F. Fruett, Multi-terminal piezo-MOSFET sensor for stress measurements in silicon, in *Proceedings of the 31st Symposium on Integrated Circuits and Systems Design (SBCCI)*, 2018, pp. 1-6.

[17]. W. D. Driel, O. Pyper, C. Schumann, Sensor Systems Simulations: From Concept to Solution, *Springer*, Cham, 2020.

[18]. Q. Zhang, Y. Liu, H. Li, J. Wang, et al., A review of SiC sensor applications in high-temperature and radiation extreme environments, *Sensors*, Vol. 24, Issue 23, 2024, 7731.

[19]. R. Wu, H. Chen, Y. Zhou, Y. Guo, et al., Advances in silicon carbides and their MEMS pressure sensors for high temperature and pressure applications, *ACS Applied Materials & Interfaces*, Vol. 17, Issue 18, 2025, pp. 26117-26155.

[20]. H. P. Phan, D. V. Dao, K. Nakamura, S. Dimitrijev, et al., The piezoresistive effect of SiC for MEMS sensors at high temperatures: A review, *Journal of Microelectromechanical Systems*, Vol. 24, Issue 6, 2015, pp. 1663-1677.

[21]. M. A. Fraga, H. Furlan, R. S. Pessoa, M. J. M. T. Massi, Wide bandgap semiconductor thin films for piezoelectric and piezoresistive MEMS sensors applied at high temperatures: An overview, *Microsystem Technologies*, Vol. 20, Issue 1, 2014, pp. 9-21.

[22]. G. Kumar, S. Kumar, M. Tetseo, K. Gogoi, et al., Analytical study on the SiC-MOSFET current mirror integrated MEMS pressure sensor for harsh environment applications, *Microsystem Technologies*, Vol. 31, Issue 9, 2025, pp. 2657-2667.

[23]. M. Bao, Analysis and Design Principles of MEMS Devices, *Elsevier*, Amsterdam, 2005.

[24]. T. Sugiura, N. Takahashi, N. Nakano, The piezoresistive mobility modeling for cubic and hexagonal silicon carbide crystals, *Journal of Applied Physics*, Vol. 127, Issue 24, 2020, 245105.

[25]. B. Tian, H. Shang, D. Wang, Y. Liu, et al., Investigation on piezoresistive effect of n-type 4H-SiC based on all-SiC pressure sensors, *IEEE Sensors Journal*, Vol. 22, Issue 7, 2022, pp. 6435-6441.

[26]. D. Kimoto, Characterization and modeling of SiC integrated circuits for harsh environment, PhD Thesis, *Kyoto University*, Kyoto, 2017.

[27]. S. Tanaka, K. Rajanna, T. Abe, M. Esashi, Deep reactive ion etching of silicon carbide, *Journal of Vacuum Science & Technology B*, Vol. 19, Issue 6, 2001, pp. 2173-2176.

[28]. Q. Wang, R. Zhang, Q. Chen, R. Duan, A review of femtosecond laser processing of silicon carbide, *Micromachines*, Vol. 15, Issue 5, 2024, 639.

[29]. S. Das, Y. Zheng, A. Ahyi, M. A. Kuroda, et al., Study of carrier mobilities in 4H-SiC MOSFETs using Hall analysis, *Materials*, Vol. 15, Issue 19, 2022, 6736.

[30]. R. R. Rao, S. Balaji, K. Matocha, V. Tilak, An approach to model temperature effects of interface traps in 4H-SiC, *Materials Science Forum*, Vol. 556, 2007, pp. 497-500.

[31]. S. Das, D. J. Lichtenwalner, S. R. Stein, S. H. Ryu, Characterization of interface trap and mobility degradation in SiC MOS devices using gated Hall measurements, *Solid State Phenomena*, Vol. 375, 2025, pp. 49-53.

[32]. S. Potbhare, Modeling and characterization of 4H-SiC MOSFETs: High field, high temperature, and transient effects, PhD Thesis, *University of Maryland*, College Park, 2008.

[33]. P. Fiorenza, F. Giannazzo, F. Roccaforte, Characterization of SiO2/4H-SiC interfaces in 4H-SiC MOSFETs: A review, *Energies*, Vol. 12, Issue 12, 2019, 2310.

[34]. H. Shang, B. Tian, D. Wang, Y. Liu, et al., Development of all-SiC absolute pressure sensor based on sealed cavity structure, *IEEE Sensors Journal*, Vol. 21, Issue 24, 2021, pp. 27308-27314.

[35]. X. Fang, W. Chen, G. Xin, Z. Libo, et al., Development of a 4H-SiC piezoresistive pressure sensor for high temperature applications, in *Proceedings of the 14th IEEE International Conference on Nano/Micro Engineered and Molecular Systems (NEMS)*, 2019, pp. 105-109.

[36]. T. Akiyama, T. Briand, N. F. Rooij, Piezoresistive n-type 4H-SiC pressure sensor with membrane formed by mechanical milling, in *Proceedings of the IEEE Sensors Conference*, 2011, pp. 222-225.

[37]. G. Wieczorek, B. Schellin, E. Obermeier, G. Fagnani, et al., SiC based pressure sensor for high-temperature environments, in *Proceedings of the IEEE Sensors Conference*, 2007, pp. 748-751.